Secondary organic aerosol 3. Urban/regional scale model of size- and composition-resolved aerosols

Robert J. Griffin,[1,2] Donald Dabdub,[3] Michael J. Kleeman,[4] Matthew P. Fraser,[5] Glen R. Cass,[6,7] and John H. Seinfeld[8]

Received 23 February 2001; revised 15 January 2002; accepted 18 January 2002; published 11 September 2002.

[1] The California Institute of Technology (CIT) three-dimensional urban/regional atmospheric model is used to perform comprehensive gas- and aerosol-phase simulations of the 8 September 1993 smog episode in the South Coast Air Basin of California (SoCAB) using the atmospheric chemical mechanism of part 1 [*Griffin et al.*, 2002] and the thermodynamic module of part 2 [*Pun et al.*, 2002]. This paper focuses primarily on simulations of secondary organic aerosol (SOA) and determination of the species and processes that lead to this SOA. Meteorological data and a gas and particulate emissions inventory for this episode were supplied directly by the South Coast Air Quality Management District. A summer 1993 atmospheric sampling campaign provides data against which the performance of the model is evaluated. Predictions indicate that SOA formation in the SoCAB is dominated by partitioning of hydrophobic secondary products of the oxidation of anthropogenic organics. The biogenic contribution to total SOA increases in the more rural eastern portions of the region, as does the fraction of hydrophilic SOA, the latter reflecting the increasing degree of oxidation of SOA species with atmospheric residence time. *INDEX TERMS:* 0305 Atmospheric Composition and Structure: Aerosols and particles (0345, 4801); 0345 Atmospheric Composition and Structure: Pollution—urban and regional (0305); 0365 Atmospheric Composition and Structure: Troposphere—composition and chemistry; *KEYWORDS:* secondary organic aerosol, biogenic aerosol, photooxidation, urban air quality

Citation: Griffin, R. J., D. Dabdub, M. J. Kleeman, M. P. Fraser, G. R. Cass, and J. H. Seinfeld, Secondary organic aerosol, 3, Urban/regional scale model of size- and composition-resolved aerosols, *J. Geophys. Res.*, *107*(D17), 4334, doi:10.1029/2001JD000544, 2002.

1. Introduction

[2] Comprehensive gas- and aerosol-phase simulations of air quality in the South Coast Air Basin of California (SoCAB) are presented for 8 September 1993, a day on which some of the highest 1-hour average ozone concentrations of 1993 in the SoCAB were observed. Simulations were performed using the California Institute of Technology (CIT) three-dimensional urban/regional air quality model. Gas-phase simulations are based on the new atmospheric chemical mechanism developed in part 1 [*Griffin et al.*, 2002] that includes representation of gas-phase chemistry leading to secondary organic aerosol (SOA) formation. Partitioning of secondary organic oxidation products to either an aqueous or an absorptive organic phase is determined using the new thermodynamic module of part 2 [*Pun et al.*, 2002]. This work represents the first attempt to simulate organic aerosol formation on a first-principles thermodynamic basis in a three-dimensional atmospheric model.

[3] Previous gas- and aerosol-phase modeling studies performed for the SoCAB using the CIT model focused primarily on the episode of 27–29 August 1987, which was part of the Southern California Air Quality Study (SCAQS). *Meng et al.* [1998] performed a full gas- and aerosol-phase simulation in which particles were both size resolved and chemically resolved. The major differences between the versions of the CIT model employed by *Meng et al.* [1998] and in the current work are described subsequently. Previous studies using the CIT model have investigated, for

[1]Department of Chemical Engineering, California Institute of Technology, Pasadena, California, USA.
[2]Now at Department of Civil and Environmental Engineering, Duke University, Durham, North Carolina, USA.
[3]Department of Mechanical and Aerospace Engineering, University of California at Irvine, Irvine, California, USA.
[4]Department of Civil and Environmental Engineering, University of California at Davis, Davis, California, USA.
[5]Department of Environmental Science and Engineering, Rice University, Houston, Texas, USA.
[6]School of Earth and Atmospheric Sciences, Georgia Institute of Technology, Atlanta, Georgia, USA.
[7]Deceased July 30, 2001.
[8]Department of Chemical Engineering and Division of Engineering and Applied Science, California Institute of Technology, Pasadena, California, USA.

0148-0227/02/2001JD000544

example, the link between ozone and particulate matter (PM) [*Meng et al.*, 1997] and the contribution of SOA to PM levels in the SoCAB [*Pandis et al.*, 1993]. *Jacobson et al.* [1996] and *Jacobson* [1997] have developed a three-dimensional model that has been applied to the 1987 SCAQS episode to simulate gas- and particle-phase air quality. Other simulations of Los Angeles gas and aerosol air quality have been reported for other episodes and using different models. *Lurmann et al.* [1997] used the Urban Airshed Model (UAM) [*Systems Applications International*, 1990a, 1990b, 1990c, 1990d, 1990e] to simulate the SCAQS episode of 24–25 June 1987 while employing the SEQUILIB inorganic thermodynamic model of *Pilinis and Seinfeld* [1987], a precursor to the thermodynamic model used by *Meng et al.* [1998]. The work also included an empirical fog model to account for the effect of fogs on gas-phase photolysis rates; fog processing of aerosols was not considered. SOA modeling work has also been performed in other areas [*Andersson-Sköld and Simpson*, 2001].

[4] In previous studies, ambient aerosols generally have been represented as an internal mixture (in which all particles of a given size have the same composition) using Eulerian grid cells (coordinates that are fixed in space). An assumed internal aerosol mixture does not require that all constituents within a given aerosol particle interact. *Kleeman et al.* [1997], however, recently developed a Lagrangian model (with coordinates that follow the trajectory of an air parcel) that treats airborne particles as an external mixture of different particle classes, defined based on the original emission source of the particle. This model has been applied to both the 28 August 1987 SCAQS episode [*Kleeman et al.*, 1997] and to data collected during the summer of 1996 in the SoCAB [*Kleeman and Cass*, 1999]. In the present study we continue to employ the internally mixed assumption, as it is sufficiently accurate for most situations and the computational demands of a full thermodynamic treatment of inorganic/organic aerosols in a three-dimensional model are inordinately large.

2. Model Description

[5] The evolution of the host Eulerian CIT model has been described in detail previously [*McRae et al.*, 1982; *McRae and Seinfeld*, 1983; *Harley et al.*, 1993, *Meng et al.*, 1998]. In application to the SoCAB, the horizontal domain of the model is an 80 by 30 grid with a resolution of 5 km; vertical resolution consists of five layers up to 1100 m above the surface. Aerosol concentrations are characterized by mass and are resolved into eight size domains with diameters ranging from 0.04 to 10 μm. Such a sectional approach is the most general and powerful approach for representing aerosol size and composition. It allows for any desired degree of size resolution and chemical speciation and is typically more computationally intensive than a modal approach, such as that used by *Binkowski and Shankar* [1995]. The aerosol is considered to be an internal mixture of elemental carbon (EC), organics, and inorganics including water. Aerosol processes not considered in the present application include coagulation, wet deposition, nonequilibrium chemical reactions that take place on aerosol surfaces, and interactions with fog and clouds.

2.1. Aerosol Thermodynamics

[6] The module Simulating Composition of Atmospheric Particles at Equilibrium 2 (SCAPE2) is used to describe the gas-aerosol partitioning of inorganic aerosol constituents [*Kim et al.*, 1993b, *Meng et al.*, 1995]. As discussed in part 2 [*Pun et al.*, 2002], the module has been modified to account for the effect of aqueous phase organic ions on the distribution of inorganic aerosol constituents. SCAPE2 is used to calculate equilibrium surface concentrations of all semivolatile inorganic species in gas-phase concentration units. These calculations are performed in a size-resolved fashion in which the composition in individual bins is used to determine bin-specific equilibrium gas concentrations. Size-specific condensation or evaporation is then driven by the difference between the calculated equilibrium surface vapor concentration and the bulk gas-phase concentration. Inorganic condensation/evaporation processes are modeled dynamically in this work except for water and carbonates, which are assumed to achieve equilibrium instantaneously. SCAPE2 allows for calculations of multicomponent inorganic activity coefficients by the Bromley, Kusik-Meissner (KM), or Pitzer methods. The KM method is used in the present work, as it has been shown that it gives the most reliable results for simulating concentrated solutions typical of nonideal ambient aerosols [*Kim et al.*, 1993a]. The Zdanovskii-Stokes-Robinson (ZSR) method is used to estimate water activities [*Robinson and Stokes*, 1965]. Temperature dependencies of equilibrium constants and relative humidities of deliquescence are also considered. In addition to water, species considered include sodium, sulfate, ammonium, nitrate, chloride, potassium, calcium, magnesium, and carbonate.

[7] Organic aerosol partitioning is driven by an instantaneous equilibrium between the gas-phase and a condensed aerosol phase (aqueous or organic), as described in part 2 [*Pun et al.*, 2002]. In the organic aerosol partitioning module, calculations are performed in a bulk mode in which the net composition of the components across all aerosol bins are summed (liquid water content and primary organic aerosol (POA) concentrations). The resulting equilibrium gas and particle concentrations are with respect to bulk properties of the aerosol. Size-resolution of secondary organics that partition between the gas phase and the condensed phase (as opposed to primary organics that reside completely in the particle phase) is determined based on available surface area within each size bin, as has been done previously [*Meng et al.*, 1998]. In the current work, it is assumed that the semivolatile secondary organic species partition to organic aerosol as opposed to any existing organic film on the ground or structures within the modeling domain because of the lack of availability of measurement data for deposition of polar organic gases. This uncertainty will be addressed as such data becomes available.

2.2. Homogeneous Nucleation

[8] New particle mass formed via homogeneous nucleation is considered only for the sulfuric acid-water system.

Based on binary nucleation of sulfuric acid and water, the threshold sulfuric acid concentration required for new particle formation, C_{crit,H_2SO_4} ($\mu g\ m^{-3}$), is given by

$$C_{crit,H_2SO_4} = 0.16 \exp(0.1T - 3.5\mathrm{RH} - 27.7), \quad (1)$$

where temperature (T) is in Kelvin and relative humidity (RH) is between 0 and 1 [*Wexler et al.*, 1994; *Meng et al.*, 1998]. If the simulated ambient gas-phase concentration exceeds this critical value, the amount in excess is transferred from the gas phase to the aerosol phase in the smallest size bin. The gas-phase concentration is accordingly set to C_{crit,H_2SO_4}. Under typical urban particle loadings, nucleation is generally not expected to occur.

2.3. Equations Governing Gas-Phase Dynamics

[9] The spatial and temporal distributions of the concentrations of gas-phase species are governed by the atmospheric convective diffusion equation, as described by *Harley et al.* [1993],

$$\frac{\partial C_i}{\partial t} + \nabla \cdot \left(\overline{\boldsymbol{V}} C_i\right) = \nabla \cdot (\boldsymbol{K} \nabla C_i) + R_i + Q_i, \quad (2)$$

where C_i is the ensemble mean concentration of species i in the gas phase, $\overline{\boldsymbol{V}}$ is the mean wind velocity vector (later shown as $\overline{\boldsymbol{V}}$ $(\boldsymbol{x}, \boldsymbol{t})$ to indicate its spatial and temporal dependence), $\boldsymbol{K}$ is the turbulent diffusivity tensor (later shown as $\boldsymbol{K}(\boldsymbol{x}, \boldsymbol{t})$), R_i is the rate of formation or removal of species i by reactions in the gas-phase, and Q_i is a source term, such as elevated point emissions. R_i is determined by the chemical mechanism used within the host model. The Caltech Atmospheric Chemistry Mechanism (CACM) described in part 1 [*Griffin et al.*, 2002] has been developed in order to predict formation of highly oxygenated secondary organic products capable of partitioning to the aerosol phase; this mechanism is used in the present study. CACM includes over 190 chemical species that participate in over 360 reactions. Currently, all emissions are treated as if they occur at ground level, meaning that Q_i is zero in this study. The surface boundary condition for solution of equation (2) sets the upward flux of each species equal to the emissions flux minus that due to dry deposition. A no-flux condition is set at the top of the domain. As described subsequently, lateral boundary conditions and initial conditions are established using measured ambient data. The use of operator splitting allows for the decoupling of the chemistry and the aerosol computations from transport calculations. Therefore, equation (2) is solved to determine C_i as a function of space and time. This vector of concentrations is then used in the inorganic and organic thermodynamic aerosol modules that determine the distribution of each species between the gas and aerosol phases.

2.4. Dry Deposition of Gas-Phase Species

[10] As described above, dry deposition of gas-phase species is used to determine surface boundary conditions for solution of the atmospheric diffusion equation. Representation of dry deposition in the CIT model is described by *Harley et al.* [1993]. A maximum dry deposition velocity, $v_{g\,max}$, is calculated in each grid cell assuming irreversible deposition,

$$v_{g\,\max} = \frac{k^2 u(z_r)}{\left[\int_{z_0}^{z_r} \varphi_m\left(\frac{z}{L}\right)\frac{dz}{z}\right]\left[2\left(\frac{Sc}{\mathrm{Pr}}\right)^{2/3} + \int_{z_0}^{z_r} \varphi_p\left(\frac{z}{L}\right)\frac{dz}{z}\right]}, \quad (3)$$

where k is von Karman's constant (0.40), $u(z_r)$ is the wind speed at the reference height z_r, z_0 is the surface roughness length, L is the Monin-Obukhov length (indicative of the stability of the boundary layer), Sc is the Schmidt number (the ratio of the momentum diffusivity to the mass diffusivity), and Pr is the Prandtl number (the ratio of the momentum diffusivity to the heat diffusivity). Here φ_m and φ_p are functions that describe momentum and heat-flux profiles in the boundary layer [*Businger et al.*, 1971]. The dry deposition velocity v_g^i of each species i is calculated from $v_{g\,max}$ and a surface resistance term

$$v_g^i = \frac{1}{\left(1/v_{g\,\max}\right) + r_s^i}, \quad (4)$$

where r_s^i is the surface resistance term for the species of interest in the grid cell of interest. Surface resistance terms vary from grid cell to grid cell because of the 32 different land-use types that exist in the SoCAB. These land-use types include, for example, urban, agricultural, forest, water, and barren land (such as beaches). Resistance terms are also affected by wind speed, atmospheric stability, and the chemical nature of the depositing molecule.

2.5. Equations Governing Aerosol Dynamics

[11] The number concentration of particles in an incremental volume of air is governed by [*Meng et al.*, 1998]

$$\begin{aligned}\frac{\partial n(m,t)}{\partial t} = &-\frac{\partial}{\partial m}[I(m,t)n(m,t)] + \frac{1}{2} \\ &\cdot \int_0^m \beta(m', m-m')n(m',t)n(m-m',t)dm' - n(m,t) \\ &\cdot \int_0^\infty \beta(m,m')n(m',t)dm' + S(m,t) - L(m,t)n(m,t),\end{aligned} \quad (5)$$

where $n(m, t)$ is the number concentration of particles at time t having total particle mass between m and $m + dm$. The total mass of the particle, m, is given as the sum of the masses (m_i) of each of the individual components. $I(m, t)$ represents the rate of change of the total mass of the particle as a result of condensation or evaporation and is given as the sum of the individual rates of change for each component (sum of dm_i/dt). The rate of coagulation between particles of mass m and those of mass m' is given as $\beta(m, m')$. $S(m, t)$ represents the source term (for example, nucleation) for particles of mass m, and the first-order removal (for example, deposition) of particles of mass m is given by $L(m, t)n(m, t)$.

[12] For most simulations of urban/regional air quality the aerosol mass distribution has been of greater interest than the aerosol number distribution. For species i, the mass

concentration distribution is defined as $q_i(m, t) = m_i n(m, t)$, and the total aerosol mass concentration distribution function, $q(m, t)$, is defined as the sum of all q_i and is equal to the product of m and $n(m, t)$. The normalized growth (or evaporation, if it is negative) rate of species i, H_i, in a particle of given mass m is defined by

$$H_i(m,t) = \frac{1}{m}\frac{dm_i}{dt}, \tag{6}$$

where the total growth/evaporation rate (H) of the particle is given by the sum of the individual H_i for all components of the particle.

[13] In most urban and regional modeling applications focusing on aerosol mass concentrations, coagulation can be neglected [*Wexler et al.*, 1994]. Thus, the general equation governing the mass distribution of species i in the aerosol phase becomes

$$\frac{\partial q_i(m,t)}{\partial t} = H_i(m,t)q(m,t) - \frac{\partial}{\partial m}[mq_iH] + m_iS(m,t) - L(m,t)q_i(m,t). \tag{7}$$

[14] Including the spatial dependence of q_i, incorporating terms for advection and turbulent mixing, and transforming m to a normalized particle diameter ($\mu = \ln(D_p/D_{p0})$, where D_p is the particle diameter and D_{p0} is the smallest diameter modeled in the size domain), results in the basic governing equation for the aerosol portion of the three-dimensional atmospheric model,

$$\frac{\partial p_i(\mu,\boldsymbol{x},t)}{\partial t} = -\left(\overline{\boldsymbol{V}}(\boldsymbol{x},t) - V_s(\mu)\boldsymbol{k}\right)\cdot\nabla p_i + \nabla\cdot\boldsymbol{K}(\boldsymbol{x},t)\nabla p_i + H_i(\mu,\boldsymbol{x},t)p(\mu,\boldsymbol{x},t) - \frac{1}{3}\frac{\partial}{\partial\mu}[Hp_i] + S_i(\mu,\boldsymbol{x},t) - L(\mu,\boldsymbol{x},t)p_i, \tag{8}$$

where $p_i(\mu, \boldsymbol{x}, t) = (dm/d\mu)q_i$, $\boldsymbol{x}$ is the spatial coordinate vector, $V_s(\mu)$ is the particle settling velocity, and $\boldsymbol{k}$ is the unit vector in the vertical direction.

[15] The growth/evaporation rate of species i is given by [*Wexler et al.*, 1994]

$$H_i(m,t) = \frac{1}{m}\frac{dm_i}{dt} = \frac{2\pi D_p D_i}{m}\frac{C_{\infty,i} - C_{s,i}}{\frac{2\lambda}{\alpha_i D_p} + 1}, \tag{9}$$

where D_i is the molecular diffusivity of species i in air, λ is the mean free path of air, α_i is the accommodation coefficient for species i on the aerosol, and $C_{\infty,i}$ and $C_{s,i}$ are the concentrations of i in the bulk and at equilibrium at the particle surface, respectively. For inorganic species, surface vapor concentrations are estimated using the thermodynamic routine SCAPE2. Concentrations of organic species in each phase are calculated thermodynamically according to the equilibrium module described in part 2.

[16] At the ground surface, the balance between emission and dry deposition represents a boundary condition for equation (8). This condition is typically expressed with a deposition velocity, V_d, where $V_d = F/C(z_r)$. F is the downward flux caused by deposition, and $C(z_r)$ is the concentration at reference height z_r (typically 10 m). The flux of species i is given by [*Wesely*, 1989]

$$F_i = [K_{zz}(z) + D_i](dC_i(z)/dz) + V_sC_i(z), \tag{10}$$

where K_{zz} is the zz-component of the eddy diffusivity tensor. Dry deposition of particle-phase species is handled differently than that of gas-phase species because of the need to include deposition due to gravitational settling. The particle deposition velocity, V_d, is then used in a manner similar to $v_{g\,max}$ in equation (4) to calculate overall deposition. Again, deposition to different land-use categories is considered within the CIT model.

2.6. Solution of Advection and Condensation/Evaporation Equations

[17] Two new numerical algorithms have been implemented into the CIT model to solve the hyperbolic advection and condensation/evaporation equations in the model. Previously, both of these equations had been solved using Bott's method, as described by *Dhaniyala and Wexler* [1996]. The Quintic Splines Taylor Series Expansion (QSTSE) algorithm, an Eulerian scheme that uses Quintic splines to calculate derivatives in the spatial domain and a Taylor series expansion to progress in time, is used to solve the advection equation [*Nguyen and Dabdub*, 2001]. Results have shown that the QSTSE algorithm maintains high accuracy while providing significant decreases in computation time over previously used methods. The Partitioned-Flux Integrated Semi-Lagrangian Method (PFISLM) is used to solve both the hyperbolic (redistribution) and growth portions of the condensation/evaporation equation [*Nguyen and Dabdub*, 2002]. PFISLM is a super set of flux integrated semi-Lagrangian methods. The unique feature of PFISLM is that it uses both semi-Lagrangian and Lagrangian fluxes in order to increase the resolution of bins while aerosol computations are being performed. First, the mass that is evacuated by the semi-Lagrangian position is used to create a new bin interface at the receiving neighbor. The new bin interface is created so that mass is conserved: the mass that is evacuated by the semi-Lagrangian position must equal the mass that is gained by the bin interface and Lagrangian position by continuity. It is possible to divide the original bin into one, two, or three partitions depending on the divergence of the condensation rate. Research has shown [*Nguyen and Dabdub*, 2002] that the higher bin resolution generated increases significantly the accuracy of the numerical solution to the condensation/evaporation equation. In particular, PFISLM surpasses the accuracy of fourth-order Bott solver [*Dhaniyala and Wexler*, 1996], which uses only the semi-Lagrangian position. PFISLM is positive definite, peak retentive, and mass conservative.

3. Required Model Input: Emissions and Meteorology

[18] For the temporally and spatially resolved aerosol emissions inventory, the particle phase is apportioned into eight size sections, and the appropriate mass of each species is placed into the proper size bin at each time and location [*Fraser et al.*, 2000]. Aerosol species include EC, sodium, chloride, ammonium, sulfur (in two oxidation states), nitrate,

Table 1. Particulate Emissions by Species and Size (metric ton day^{-1}) in the SoCAB on 8 September 1993

Section	1	2	3	4	5	6	7	8	Total
D_p (μm)	0.06	0.11	0.22	0.44	0.88	1.77	3.53	7.07	
EC[a]	1.2	4.1	4.2	1.1	0.6	0.5	0.9	1.5	14.1
OC[b]	4.6	6.1	6.9	4.8	3.0	4.2	11.2	20.5	61.3
Sodium ion	0.1	0.1	0.1	0.05	0.05	0.1	0.2	0.4	1.1
Chloride ion	0.2	0.2	0.2	0.1	0.1	0.1	0.2	0.3	1.4
Ammonium	0.006	0.022	0.025	0.02	0.013	0.002	0.002	0.002	0.1
Sulfur (VI)	1.2	0.6	0.6	0.6	0.5	0.3	0.7	1.4	5.9
Nitrate	0.2	0.2	0.2	0.1	0.1	0.1	0.2	0.4	1.5
Other	1.8	3.0	9.1	16.6	18.9	35.9	112.5	184.2	382.0
Metals	0	0.1	0.1	0.1	0.1	0.2	1.2	1.2	3.0
Unknown	0.3	2.0	3.2	3.2	3.3	5.5	13.0	25.7	56.2
Sulfur (IV)	0	0.006	0.009	0.009	0.019	0.021	0.034	0.034	0.1
n-Alkanes	0.1	0.023	0.022	0.013	0.012	0.021	0.1	0.1	0.4
Diacids	0.009	0.028	0.02	0.004	0.002	0.001	0.001	0.001	0.1
Oxygenated PAH	0.3	0.015	0.009	0.001	0.001	0	0.001	0.001	0.3
PAH	0.4	0.019	0.019	0.007	0.004	0.006	0.01	0.013	0.5
Cyclics	0.006	0.009	0.007	0.005	0.0004	0.007	0.014	0.024	0.1
Substituted monoaromatics	0	0	0	0	0	0	0	0	<0.0001
Aliphatic acids	0.1	0.046	0.1	0.1	0.1	0.1	0.2	0.4	1.1
Total	10.5	16.6	24.8	26.8	26.8	47.1	140.5	236.2	529

[a] EC = elemental carbon.
[b] OC = unresolved organic carbon.

metals (e.g., calcium, magnesium, and potassium), organics, and unidentified/other material. Organic particle-phase species can be further segregated into seven primary aerosol categories based on chemical analysis of samples from emission sources: *n*-alkanes, polycyclic aromatic hydrocarbons (PAH), diacids, aliphatic acids, substituted PAH, resolved polycyclic species (e.g., hopanes), and substituted monoaromatics. Unresolved organic matter (typically highly cyclic, saturated, and branched petroleum biomarkers) constitutes an eighth POA emissions group [*Rogge et al.*, 1993; *Schauer*, 1998; *Schauer et al.*, 1999a, 1999b, 2001]. Emissions inventories (both particle and gas) were obtained from the South Coast Air Quality Management District (SCAQMD). Summaries of daily particle-phase emissions for 8 September 1993 are given in Table 1 by species and size. Initial and boundary conditions for PM are established based on observed aerosol size and composition distributions obtained in the SCAQS sampling campaign [*John et al.*, 1990].

[19] Because the character of the POA species affects the partitioning of the secondary organic oxidation products as described in part 2 [*Pun et al.*, 2002], representative surrogates must be chosen to represent each POA category listed above (*n*-alkanes, PAH, etc.). The surrogates used are *n*-nonacosane, benzo(ghi)perylene, butanedioic acid, octadecanoic acid, 2,6-naphthalene-diacid, 17(α)H-21(β)H-hopane, phthalic acid (1,2-benzene-diacid), and a polysubstituted decalin compound. These species are chosen based on their identified prevalence in POA emissions in the SoCAB [*Rogge et al.*, 1993; *Schauer*, 1998; *Schauer et al.*, 1999a, 1999b, 2001]. If an organic species is emitted as aerosol, it is assumed that it remains in the particle phase and is nonreactive.

[20] Species that are included in the other/unidentified category above may include arsenic, bromine, phosphorous, selenium, and silicon, which most likely have crustal sources. The mass of these other/unidentified species is found by the difference between the total gravimetric mass measured during emissions sampling and that mass which can be identified using an array of analytical techniques. Particulate water (not measured analytically) and oxygen or nitrogen associated with organics may also contribute to this category. In the analysis of the emissions, total organic carbon is reported and then converted to total organic mass. In this conversion, the total mass of organics may be underestimated, leading to some organic mass being included in the other/unidentified category. In the current study, the other/unidentified species are treated as nonvolatile components of the aerosol.

[21] A highly aggregated summary for the gas-phase emissions is given in Table 2. Hourly gas-phase emissions (point and mobile sources) for each of the model grid cells were supplied by SCAQMD. The baseline emissions inventories used for the modeling exercise were generated by the SCAQMD for 1993 as a part of the 1997 Air Quality Management Plan. The emissions inventories reflect both collected available information and projections for the automobile fleet and industrial emissions of 1993. The biogenics emissions inventory was represented using the biogenics emissions inventory developed for the late August episode of the SCAQS. It is assumed that the amount and type of vegetation located in the SoCAB in the late summer and early fall likely did not change significantly between 1987 and 1993. Mobile source emissions were generated through use of the California Air Resources Board (CARB) emissions model EMFAC-7G (available from the California Air Resources Board at http://www.arb.ca.gov/msei/mvei/mvei.htm). Gas-phase emissions are broken down into ammonia, oxides of sulfur (SO_x), oxides of nitrogen (NO_x), CO, and organic species. (Ammonia and SO_x are not shown in Table 2.) Organic species are lumped according to chemical structure and functionality, reactivity, and experimentally determined SOA forming potential. As discussed in part 1 [*Griffin et al.*, 2002], the parent organic groups include ethene (ETHE), short-chain alkenes (OLEL), long-chain alkenes (OLEH), short-chain alkanes (ALKL), medium-chain alkanes (ALKM), long-chain alkanes (ALKH), high-SOA yield aromatics (AROH), low-SOA yield aromatics (AROL), phe-

Table 2. Gas-Phase Emissions by Species and Source (metric ton day^{-1}) in the SoCAB on 8 September 1993

Category	NMOG[a]	NO_x	CO
Fuel combustion	12.4	105.7	46.9
Waste burning	0.5	1.9	2.8
Solvent use	335.2	0.3	0.2
Petroleum process (storage/transfer)	50.8	0.3	3.7
Industrial processes	21.4	5.5	0.8
Miscellaneous processes	65.9	1.0	9.3
On-road vehicles	1117.6	701.5	9236.9
Other mobile	103.7	250.0	1379.3
Other sources	119.2	0.0	0.3
Total	1826.7	1066.2	10680.1

[a] Nonmethane organic gases.

nolic aromatics (AROO), aldehydic aromatics (ARAL), acidic aromatics (ARAC), polycyclic aromatic hydrocarbons (PAH), formaldehyde (HCHO), higher aldehydes (ALD2), short-chain ketones (KETL), long-chain ketones (KETH), methanol (MEOH), ethanol (ETOH), higher alcohols (ALCH), isoprene (ISOP), low-SOA yield monoterpenes (BIOL), high-SOA yield monoterpenes (BIOH), and methyl-*tert*-butyl ether (MTBE). If only total organic emissions are known for a given source, the split among the groups is assumed based on the observed ambient data. These splits are also used to establish boundary and initial conditions (Table 3). Previous work has shown that on-road motor vehicle emissions in the SoCAB have been underpredicted significantly by the methodology used to develop spatially and temporally resolved emission patterns from SCAQMD emission inventories [*Pierson et al.*, 1990; *Fraser et al.*, 1998]. Therefore, hot exhaust emissions of volatile organics and CO from light duty vehicles were increased by a factor of 3 [see, e.g., *Harley et al.*, 1993; *Fraser et al.*, 2000]. Ammonia emissions are based upon the inventory of *Gharib and Cass* [1984].

[22] Meteorological parameters include relative humidity, temperature, wind, ultraviolet radiation, total solar radiation, and mixing height. Relative humidity is important as it determines, at a given time, the amount of gas-phase water present, which can participate in a number of reactions, including the reaction with $O(^1D)$ to form the hydroxyl radical and with N_2O_5 to form nitric acid, HNO_3. Relative humidity also determines the amount of water that partitions to the aerosol phase at equilibrium. Temperature is a key variable in that it affects the kinetics of gas-phase reactions, the equilibrium constants and relative humidities of deliquescence of the inorganic species, and the partitioning of organic species explicitly and implicitly through its effect on vapor pressure.

[23] Meteorological parameters were obtained from a variety of sources. Hourly observations of surface wind speed and direction were taken at 21 sites by the California Irrigation Management Information Service (CIMIS) and at 32 sites by the SCAQMD. Temperature and relative humidity data were recorded at the 21 CIMIS sites, at 13 of the SCAQMD sites, and at 52 sites operated by the National Climatic Data Center. Total solar radiation was monitored by SCAQMD at six sites and by CIMIS at its 21 sites. Ultraviolet radiation was measured at one site in Central Los Angeles by SCAQMD. Hourly gridded fields for these types of data were made using the methodology described by *Harley et al.* [1993]. Inversion base height and wind aloft were inferred from upper air measurements made daily by SCAQMD in West Los Angeles at 0500 PST and by CARB in Claremont between 0600 and 1400 PST. *Winner and Cass* [1999] demonstrate the method used for creating mixing depth fields from such data.

[24] In this study, it was determined that the traditional method used to calculate vertical eddy diffusivities in the CIT model underpredicts these parameters at the low wind speeds characteristic of this episode, as judged by unrealistically high simulated concentrations at night of both tracer pollutant and secondary species in the majority of locations throughout the SoCAB. The current methodology for calculating vertical eddy diffusivities does not take into account the effects of urban heat islands and mechanical mixing near roadways. Therefore, to achieve more realistic concentrations during the evening hours, vertical eddy diffusivities were increased by enforcing a minimum wind speed (2.5 m s^{-1}) and stability class (slightly unstable). These changes promote mixing up to the height of the inversion layer but were not propagated to other processes such as advection and deposition.

4. Numerical Solution of the Governing Equations

[25] Operator splitting [*McRae et al.*, 1982] is used in the CIT model to solve the governing gas and aerosol conservation equations. This is carried out according to the order $T_xT_yT_{z,c}T_aT_yT_x$ where T_x, T_y, $T_{z,c}$, and T_a represent the operators of transport in the x-direction, transport in the y-direction, transport in the z-direction and gas-phase chemistry, and aerosol dynamics, respectively.

[26] The host CIT model is designed to solve numerically for spatial advection and diffusion terms for transport of gas-phase species, and the same techniques are applied for aerosols. Upon completion of a time step for the gas-phase mechanism, the aerosol operator is called and solved as discussed above. The aerosol operator determines the dynamic transport of all species except water, carbonates, and organics between the gas and aerosol phases. The excepted species are assumed to achieve equilibrium instantaneously. During these calculations, mass is conserved. The time step for the aerosol operator is determined by calculat-

Table 3. Assumed Distribution of Nonmethane Organic Gases (NMOGs) When Speciation is Unknown

Species i	Land Factor, ppb_i per ppm C NMOG	Ocean Factor, ppb_i per ppmC NMOG
ETHE	0.0436	0.0058
ALKL	0.4551	0.1139
ALKM	0.1113	0.0225
ALKH	0.0015	0.0000
OLEL	0.1640	0.0028
OLEH	0.0014	0.0000
AROL	0.1323	0.0000
AROH	0.0999	0.0074
AROO	0.0010	0.0000
PAH	0.0345	0.0000
ISOP	0.0028	0.0000
BIOL	0.0021	0.0000
BIOH	0.0021	0.0000

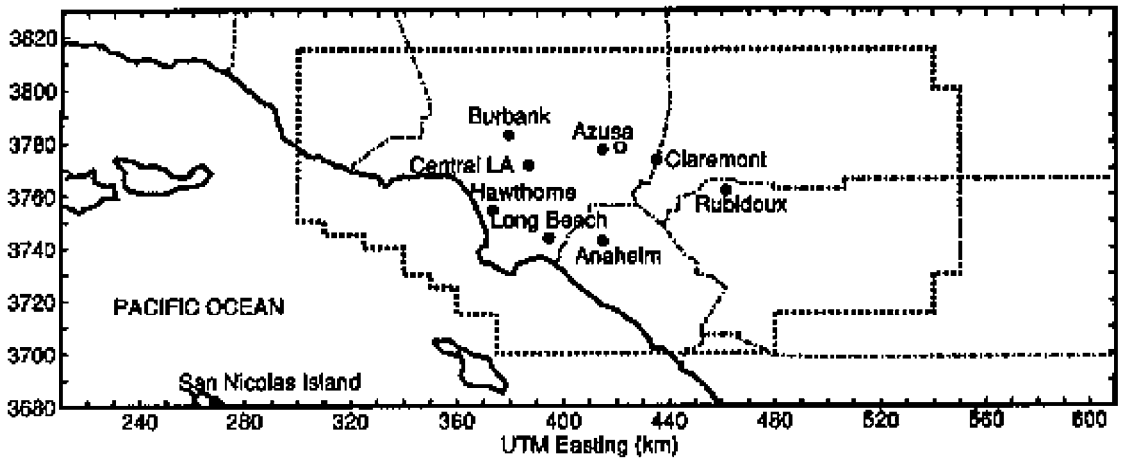

Figure 1. The South Coast Air Basin of California showing Central Los Angeles, sampling locations during the 1993 smog episode, and other suburbs for reference.

ing the characteristic times for mass transfer of each species in each size section while maintaining the stability of the solution of hyperbolic equations. The smallest of these times is then used if it is less than the maximum time step chosen during development of SCAPE2. Once the cumulative time of operation for the aerosol operator is equal to a time step of the gas-phase chemical mechanism, the transport calculations are performed.

[27] Aerosols are size-resolved based on a sectional approach; eight discrete size bins are used in the current application. The minimum diameter specified is 0.04 μm, and the maximum is 10 μm. By establishing equidistant spacing on a logarithmic scale in particle diameter, particles are sectioned into six bins that are smaller than 2.5 μm in diameter (fine mode) and two bins that are larger (coarse mode). If particles grow to sizes larger than 10 μm, their diameters are reduced to 10 μm, and the number concentration in the largest size bin is increased so that aerosol mass concentration is conserved. The opposite is done if particles shrink to sizes below 0.04 μm; the diameters of such particles are increased to 0.04 μm with a corresponding decrease in aerosol number concentration in the smallest size bin. Because aerosol particle number concentrations at the extremes of the size distribution are relatively small, the effect on population dynamics of forcing the particles to remain within the range of 0.04–10 μm while conserving mass is minimal.

5. Simulation of the 8 September 1993 Smog Episode in the SoCAB

[28] A specialized monitoring campaign was performed from 28 August to 13 September in the SoCAB during the summer of 1993 [*Fraser et al.*, 1996], the goal of which was to identify numerous individual organic species in both the gas and aerosol phases; the current study focuses on 8 September. Numerous monitoring sites were operated during the study (Figure 1). One site was located on San Nicolas Island, upwind of the Los Angeles basin, observations at which were used to establish upwind boundary conditions. Sites located within the greater Los Angeles area were chosen to represent different characteristic source regions of the SoCAB. Central Los Angeles is the hub of the region's freeway system, experiencing intense primary emissions from automobiles as well as some secondary photochemistry. Downwind locations Azusa and Claremont experience high levels of secondary pollutants. Continuous 4-hour aerosol samples were collected at each of these locations every 6 hours. Gas-phase species, such as NO, NO_2, O_3, CO, and SO_2, were also monitored hourly by the SCAQMD at 31 monitoring sites located throughout the SoCAB.

[29] During the study, meteorological conditions were controlled by the development of a high-pressure system over the air basin. The episode was characterized by a strong temperature inversion aloft that strongly limited the extent of vertical mixing. Sunny and hot conditions were conducive to intense photooxidation, with peak temperatures in the eastern portion of the basin exceeding 40°C. Slight onshore winds typically developed in the afternoon, minimally increasing transport of material inland and resulting in slightly foggy conditions in the morning.

[30] Because simulation of gas-phase concentrations has already been addressed in part 1 [*Griffin et al.*, 2002], only brief consideration will be given here. Temporal profiles of observed (solid symbols) and predicted (open symbols) ozone (triangles) and NO_2 (circles) for Azusa are given in Figure 2. As seen in Figure 2, CACM and the CIT model predict the temporal behavior of these species at this location with accuracy that is generally consistent with that of previous SoCAB simulations (see part 1). The missing NO_x peak in the morning is most likely a result of inaccuracies in the emission inventory and probably leads to the underprediction of peak ozone. The temporal profiles of the simulated (open symbols) and observed (solid symbols) concentrations of MGLY, which represents dicarbonyls that result from ring-breaking reactions of aromatics, are shown in Figure 3 for Azusa and Central Los Angeles. While MGLY is accurately predicted in the morning and evening (generally within 1 ppb), peak midday concentrations are underpredicted by a factor of 2–3. However, the temporal peak in MGLY is well represented, as it is by *Fraser et al.* [2000].

[31] Selected aerosol simulations are shown in Figures 4, 5, and 6. While the majority of the results presented here

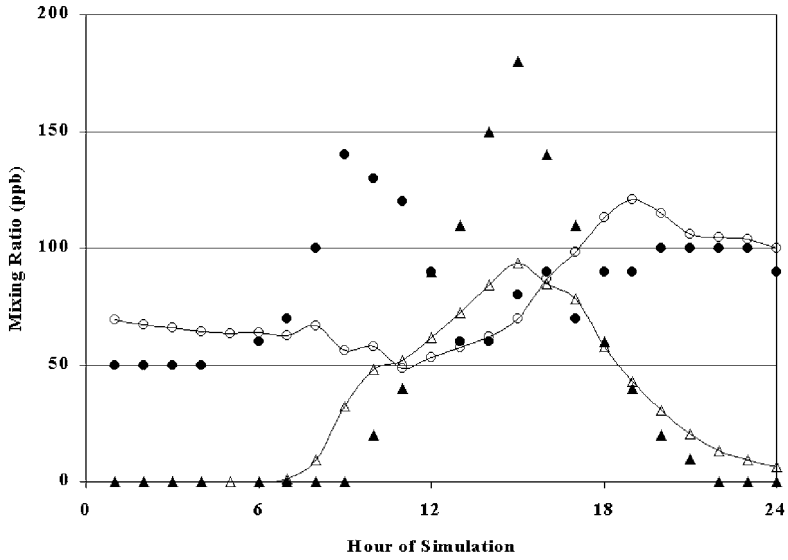

Figure 2. Predicted (open symbols) versus observed (solid symbols) NO_2 (circle) and O_3 (triangle) mixing ratios for Azusa for 8 September 1993.

will focus on SOA, Figure 4 shows simulated (open symbols) and observed (solid symbols) ammonium (circle) and nitrate (triangle) 4-hour average aerosol mass concentrations for Azusa. It is seen that nitrate levels tend to be underpredicted by a factor of 2–3 in earlier parts of the day and overpredicted by approximately 25% later. Ammonium aerosol concentrations are accurately represented in the morning and afternoon (within 1 $\mu g\ m^{-3}$) but are overpredicted by less than a factor of 2 in the evening. Simulations of the 24-hour average (the basis for ambient air quality standards available from the United States Environmental Protection Agency at www.epa.gov/airs/criteria.html) concentrations for ammonium and nitrate aerosol can also be compared to the observed 24-hour average concentrations. Both the simulated 24-hour average ammonium concentration (by less than a factor of 2) and the simulated 24-hour average nitrate concentration (by approximately 15%) in Azusa are overpredicted.

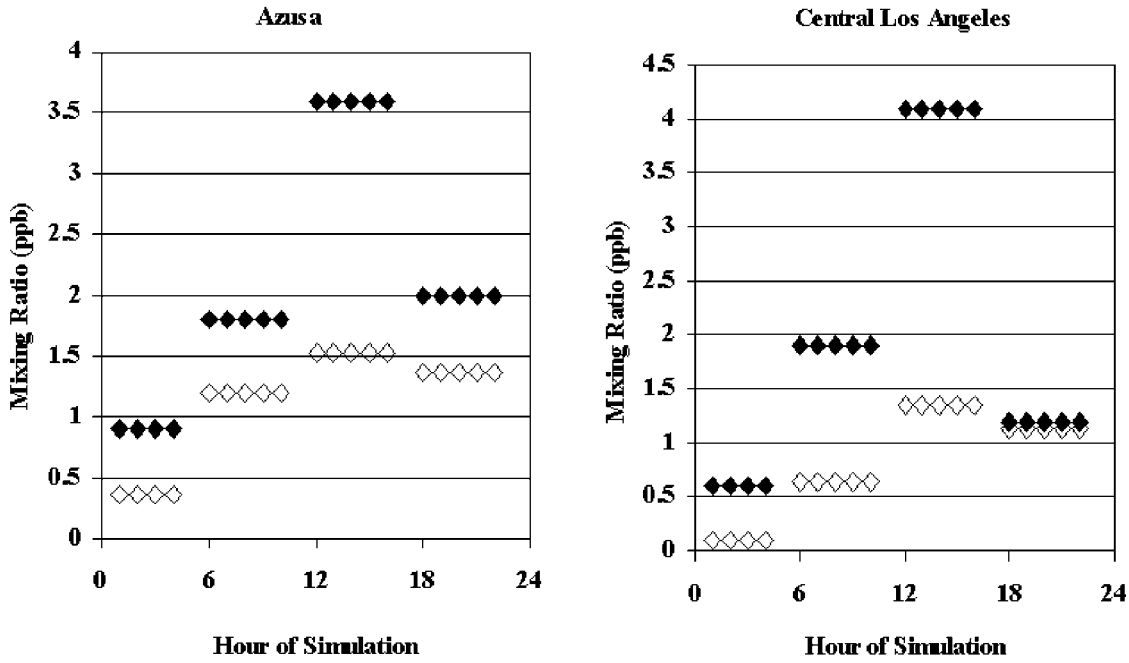

Figure 3. Predicted (open symbols) versus observed (solid symbols) MGLY 4-hour average mixing ratios for Azusa (left) and Central Los Angeles (right) for 8 September 1993.

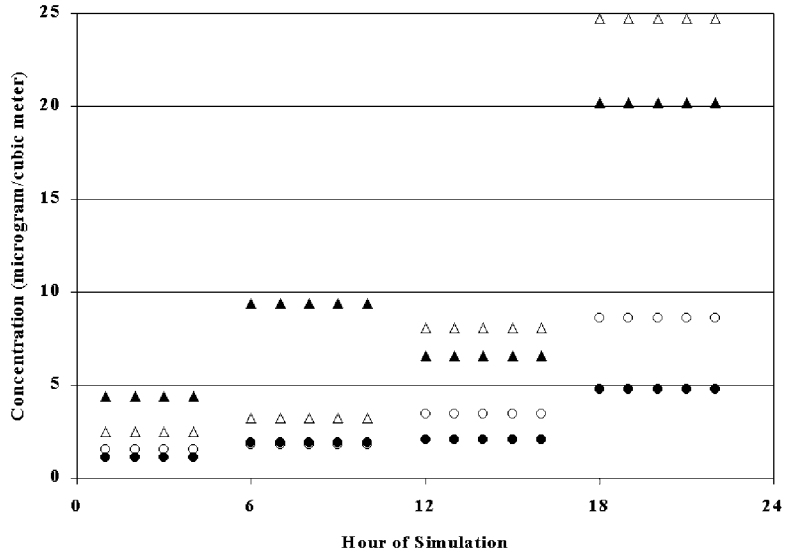

Figure 4. Predicted (open symbols) total ammonium (circle) and nitrate (triangle) concentrations ($\mu g\ m^{-3}$) versus observed (solid symbols) concentrations for Azusa for 8 September 1993.

[32] Figure 5 shows simulated (open symbols) total organic aerosol mass concentrations at Central Los Angeles (an upwind site) and Claremont (a downwind site) versus observed concentrations (solid symbols). Total organic aerosol mass is shown because of the inability of field measurements to distinguish between POA and SOA. Figure 5 indicates underprediction of the organic aerosol mass in a downwind location in the early part of the day; the most plausible explanation is that the particulate emissions inventory does not accurately reflect emissions of POA that impact this location. Other possible explanations (for example, inadequate initial conditions or gas-phase chemistry) have been eliminated using model diagnostic studies. Conversely, the organic aerosol mass concentration is overpredicted in the upwind location at night; in this location, it is believed that inaccurate simulation of nighttime turbulent mixing is responsible for the overprediction due to the fact that this overprediction at night is not species specific, as discussed earlier. These trends have been observed in simulations of aerosol concentrations in similar locations in

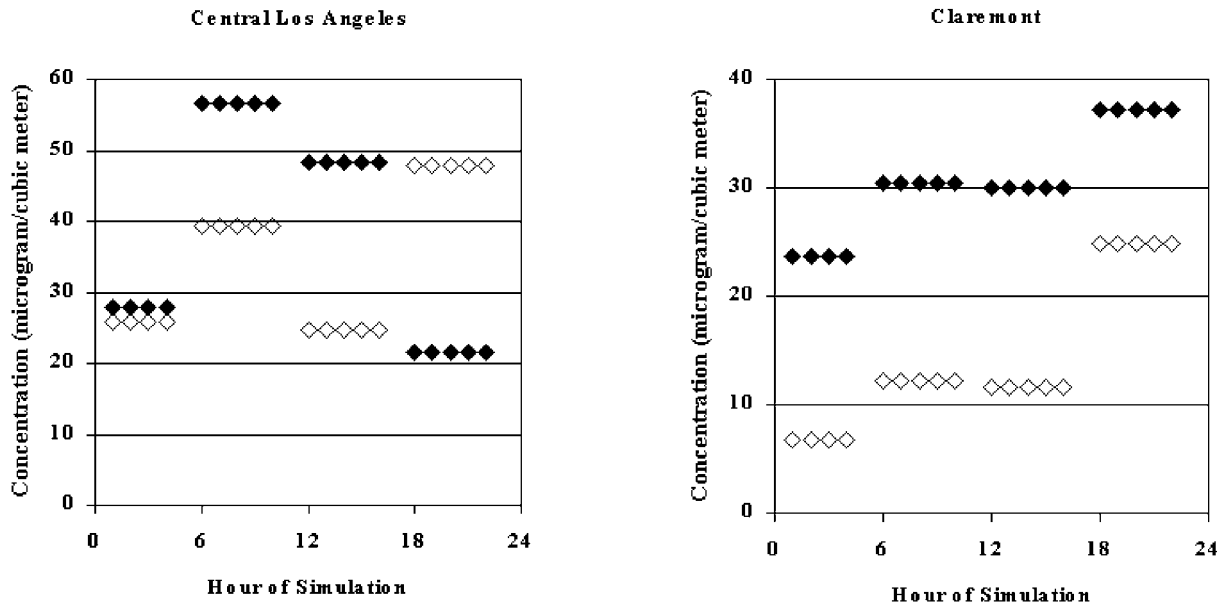

Figure 5. Predicted (open symbols) total 4-hour average organic aerosol concentrations ($\mu g\ m^{-3}$) versus observed (solid symbols) concentrations for Central Los Angeles (left) and Claremont (right) for 8 September 1993.

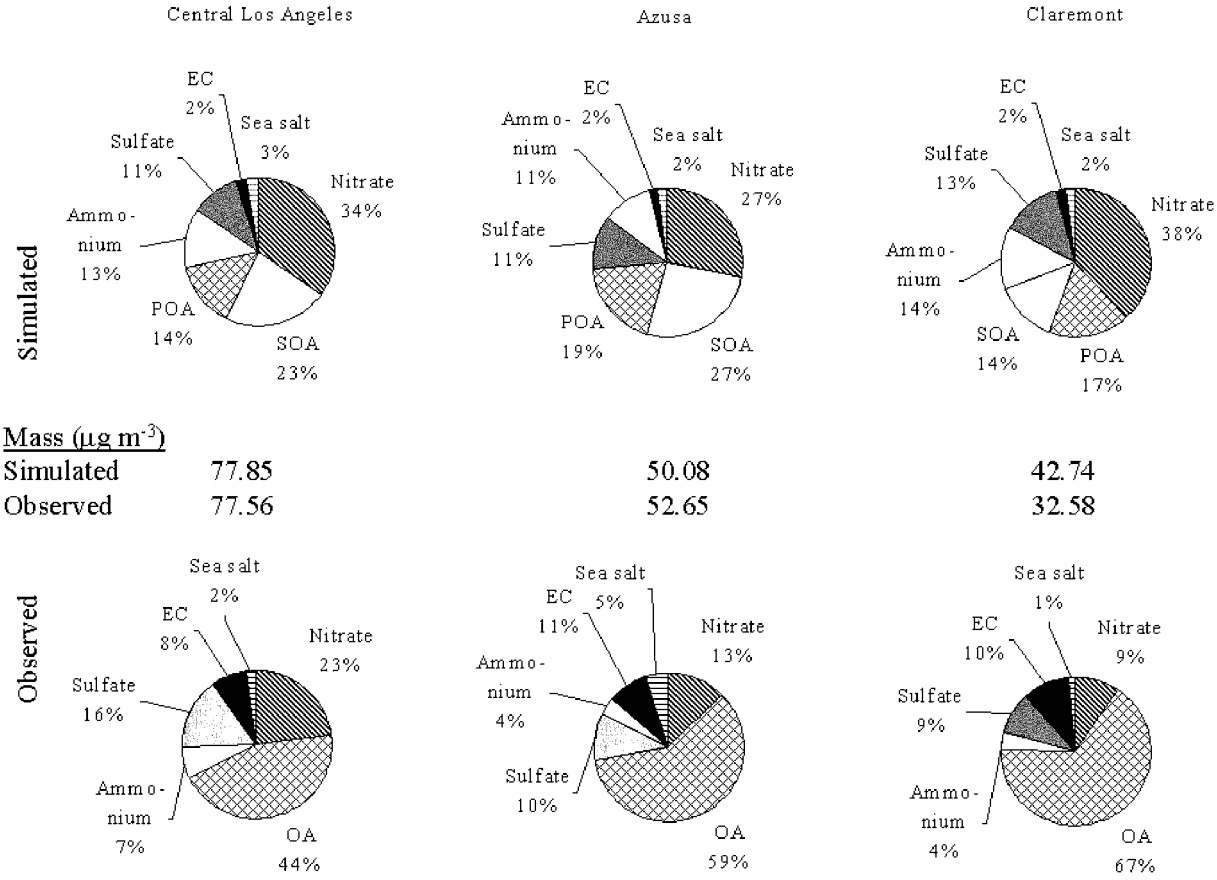

Figure 6. Predicted versus observed (4-hour average between 1200 and 1600) aerosol mass composition for Central Los Angeles, Azusa, and Claremont on 8 September 1993. The model categories metals, carbonates, water, and other inorganics are not included. Total mass concentrations given are only representative of the species shown.

the SoCAB. Simulations of the 24-hour average for organic aerosol are within 50% of the observed averages. Observed organic aerosol mass concentrations shown in Figure 5 are adapted from organic carbon aerosol data presented by *Fraser et al.* [2000] by multiplying by a factor of 1.4 [*Gray et al.*, 1984] to account for noncarbon mass associated with organics.

[33] Figure 6 shows the simulated and observed (4-hour average between 1200 and 1600) aerosol mass and composition at Central Los Angeles, Azusa, and Claremont on 8 September 1993. Total aerosol composition and mass are predicted and observed to be dependent on location. Total mass concentrations of the species shown are consistent with observations, but this result may be coincidental because individual species exhibit over and/or underpredictions.

[34] In each location, aerosol nitrate is predicted to be the most prevalent individual species, followed by organics, ammonium or sulfate, primary EC, and sea salt. In Central Los Angeles and Azusa, total organic aerosol concentration is predicted to be greater than nitrate aerosol concentration. Water, carbonates, metals, and other inorganics are not included in this composition distribution. In comparing observed to simulated compositions, it should be pointed out that in all three locations, simulated organic aerosol contributions to mass are less than those observed. Simulated nitrate and ammonium aerosol contributions are both greater than those observed despite NO_x being underpredicted in the morning hours in some locations (Figure 2). These trends are consistent with the temporal simulations presented in Figures 4 and 5. Simulated sulfate (within 5%) and sea salt (within 3%) contributions to mass are consistently represented when compared to observations. The contribution of EC is underrepresented in simulations; given the spatial consistency in this underprediction, the most plausible explanation for this underprediction is an inaccuracy in the emissions inventory.

[35] The simulated contribution of organic aerosol to total particulate levels is greatest in Azusa (46%) and smallest in Claremont (31%). The distribution of organic aerosol between secondary and primary varies between locations as well, with SOA reaching its peak percentage in Central Los Angeles (62% of total organic aerosol) and minimum percentage in Claremont (45% of total organic aerosol). The contribution of SOA to overall organic aerosol is expected to be significantly less during times of peak POA emissions.

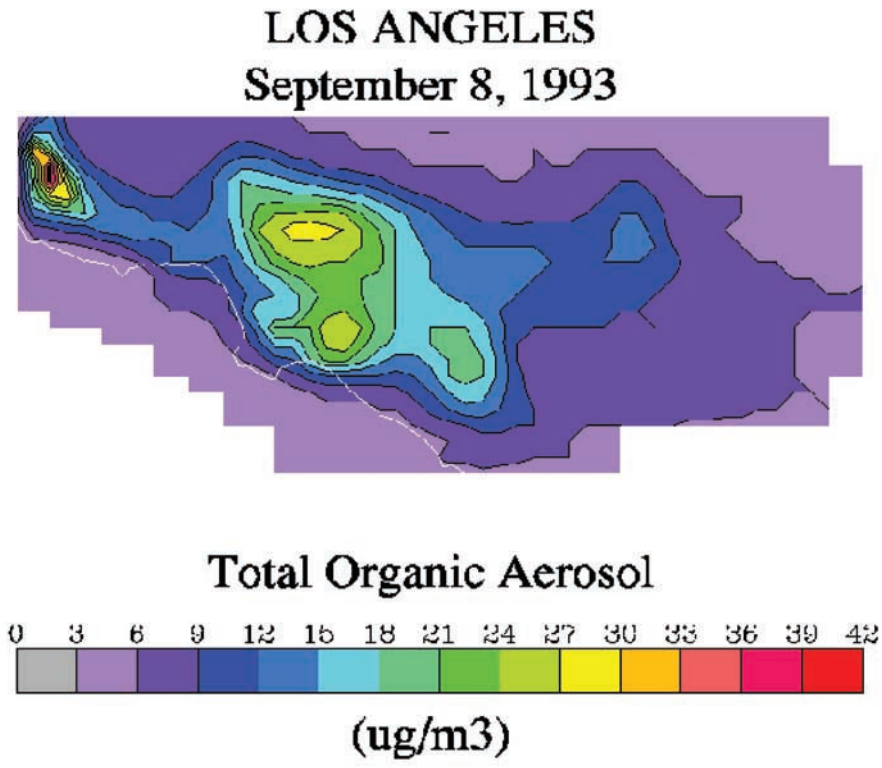

Figure 7. Predicted spatial distribution of organic aerosol PM in the SoCAB at 1400, 8 September 1993.

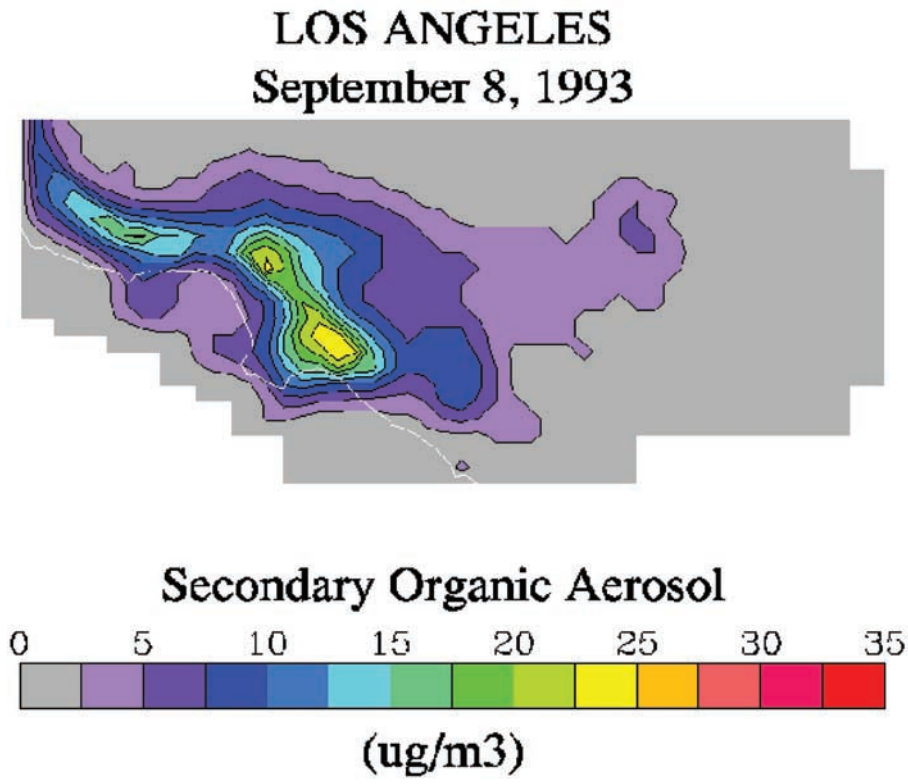

Figure 8. Predicted spatial distribution of SOA PM in the SoCAB at 1200, 8 September 1993.

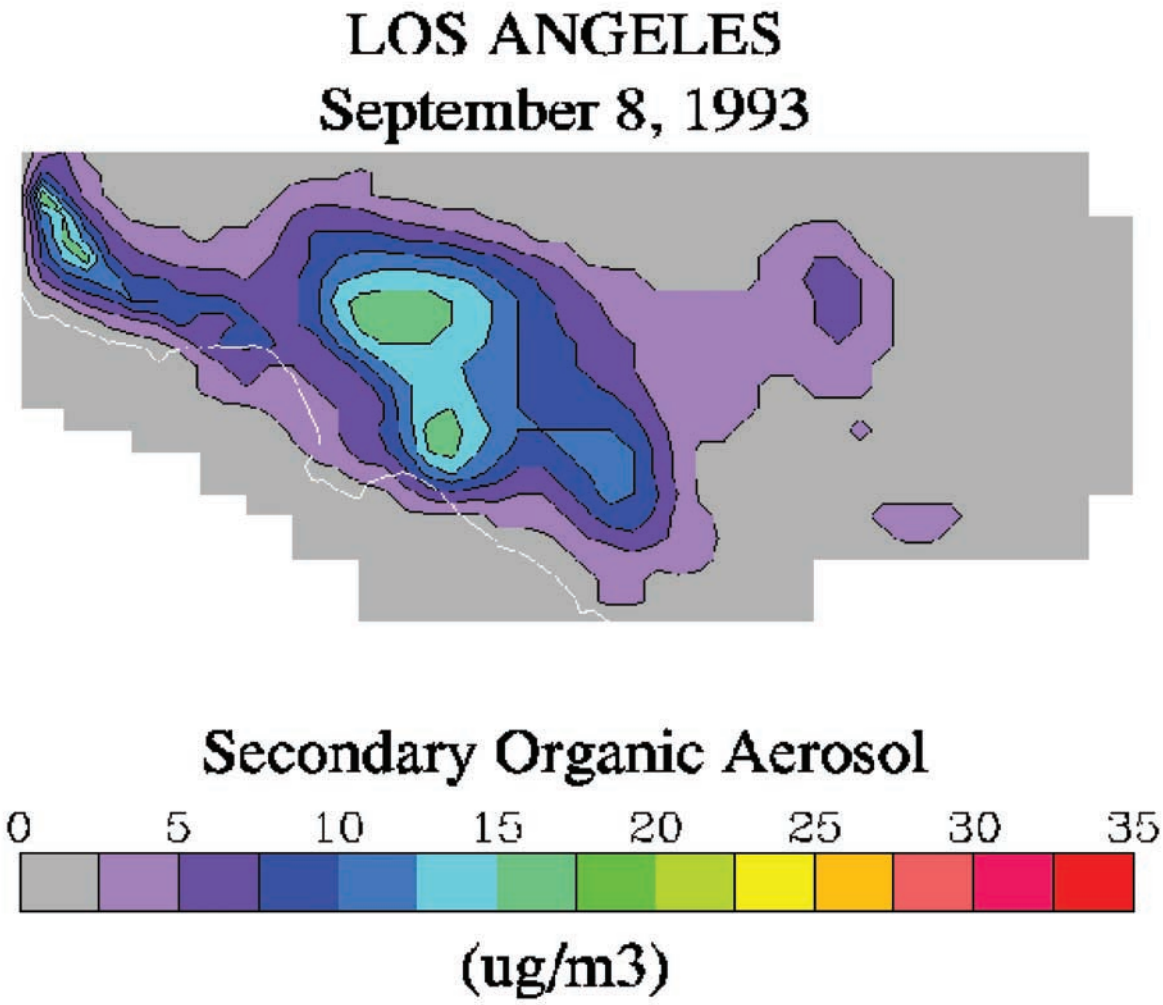

Figure 9. Predicted spatial distribution of SOA PM in the SoCAB at 1400, 8 September 1993.

[36] Figure 7 shows simulated surface-level total organic PM concentrations throughout the SoCAB at 1400 on 8 September 1993, and Figures 8 and 9 show the corresponding predictions for SOA at 1200 and 1400, respectively. Concentrations range from 4 to 40 $\mu g\ m^{-3}$ in the total organic aerosol case and from less than 0.5 to 25 $\mu g\ m^{-3}$ and from less than 0.5 to 17 $\mu g\ m^{-3}$, respectively, for the two SOA plots. Figures 7–9 indicate that SOA is predicted to contribute a significant fraction by mass of the total organic aerosol throughout the SoCAB in this episode. Organic aerosol concentrations are predicted to be highest in areas downwind that experience both secondary aerosol formation and significant transport of aerosol species from upwind locations with large sources of primary aerosol. Comparison of Figures 8 and 9 shows the expected movement inland and dilution of the peak of predicted SOA concentrations as the simulation advances in time. The aerosol concentration peaks exhibited in the top left corners of Figures 7, 8, and 9 are a result of the very low mixing heights predicted during this episode in the northwest section of the SoCAB.

[37] Table 4 shows the contributions to simulated SOA concentrations of anthropogenic and biogenic precursors and the hydrophobic and hydrophilic mechanisms of SOA formation described in part 2 [*Pun et al.*, 2002] at 1400 on 8 September 1993 in Central Los Angeles, Azusa, and Claremont. Anthropogenic SOA is shown to be the dominant contributor to total SOA in each of these locations (98.3%, 96.9%, and 92.7% by mass, respectively); however, it should be noted that the contribution of anthropogenic species to SOA decreases with downwind location. Biogenically derived SOA is most important in the eastern half of the SoCAB, as plant cover increases in the SoCAB going from upwind to downwind locations. Table 4 also exhibits that the dominant formation route for SOA in the SoCAB is via hydrophobic partitioning. SOA formed by this mecha-

Table 4. Predicted Percent Contribution to SOA Formation of Different Sources and Formation Mechanisms in Three Locations in the SoCAB

	Central Los Angeles	Azusa	Claremont
Anthropogenic	98.3	96.9	92.7
Biogenic	1.7	3.1	7.3
Hydrophobic	84.0	77.3	64.6
Hydrophilic	16.0	22.7	35.4

nism is estimated to contribute 84.0%, 77.3%, and 64.6% by mass to SOA in Central Los Angeles, Azusa, and Claremont, respectively, indicating that the hydrophilic mechanism becomes more important in the eastern portion of the SoCAB. This is partly due to the fact that biogenically derived SOA in the SoCAB shows more affinity for the aqueous phase than SOA derived from anthropogenic emissions; as discussed above, the eastern half of the SoCAB is more affected by emissions of biogenic SOA precursors. It should also be noted that the contribution of anthropogenically derived SOA formed via the hydrophilic mechanism increases relative to the hydrophobic mechanism going from upwind to downwind locations. Tertiary and quaternary oxidation products formed in higher concentrations in downwind locations are expected to be of a more oxidized nature, increasing their tendency to partition to the aqueous aerosol phase.

6. Discussion/Conclusions

[38] This series of three papers is devoted to developing a first-principles approach to the atmospheric modeling of secondary organic aerosol (SOA). The expanded gas-phase chemical mechanism has been formulated to predict the formation of classes of organic compounds that have been identified in or are likely to be constituents of ambient aerosol. The thermodynamic equilibrium module predicts the gas/particle partitioning of organics, inorganics, and water based on dividing the organic species into hydrophobic and hydrophilic fractions. Each of these modules has been integrated into the three-dimensional urban/regional CIT model and applied to simulate the 8 September 1993 smog episode in the South Coast Air Basin of California (SoCAB). This work presents for the first time atmospheric simulations of the formation of SOA on a molecular basis. As more is learned about the molecular constituency of organic aerosols, the actual classes of surrogate compounds used may change, but the framework presented in these three papers should stand as a foundation for predicting SOA formation.

[39] A system as complex as the gas-particle laden urban atmosphere is characterized by a large number of parameters and inputs, not the least of which are the basic gaseous and particulate emissions that drive the system. In addition, the current work indicates the impact that the parameterization of vertical diffusion has on predicted concentrations. Because of uncertainties inherent in these inputs, simulations of this system, even for a relatively well-characterized region like the SoCAB, cannot be expected to, and indeed do not, always match observations one-to-one. What one seeks are simulations that exhibit the correct physics and an understanding of why predictions do not match observations, when such a match does not occur. Detailed sensitivity studies often provide a means to assess these issues; limited diagnostic model runs aimed at eliminating potential causes of mismatches between predictions and observations have been performed over the course of this work, but space does not permit their detailed presentation here. Future work will continue to explore the properties of the thermodynamic partitioning module and the sensitivity of SOA levels to reductions in precursor emissions both in the SoCAB and in other regions.

[40] **Acknowledgments.** This work was funded by the United States Environmental Protection Agency under grant R826371-01, by the State of California Air Resources Board under contract 98-314, and by the Electric Power Research Institute. The simulations were performed by the Aeneas supercomputer at the University of California, Irvine. Although the research described in this article has been funded in part by the U. S. Environmental Protection Agency's STAR program through grant R826371-01, it has not been subjected to any EPA review and therefore does not necessarily reflect the views of the Agency, and no official endorsement should be inferred.

References

Andersson-Sköld, Y., and D. Simpson, Secondary organic aerosol formation in northern Europe: A model study, *J. Geophys. Res.*, *106*, 7357–7374, 2001.

Binkowski, F. S., and U. Shankar, The regional particulate matter model, 1, Model description and preliminary results, *J. Geophys. Res.*, *100*, 26,191–26,209, 1995.

Businger, J. A., J. C. Wyngaard, Y. Izumi, and E. F. Bradley, Flux-profile relationships in the atmospheric surface layer, *J. Atmos. Sci.*, *28*, 181–189, 1971.

Dhaniyala, S., and A. S. Wexler, Numerical schemes to model condensation and evaporation of aerosols, *Atmos. Environ.*, *30*, 919–928, 1996.

Fraser, M. P., D. Grosjean, E. Grosjean, and G. R. Cass, Air quality model evaluation data for organics, 1, Bulk chemical composition and gas/particle distribution factors, *Environ. Sci. Technol.*, *30*, 1731–1743, 1996.

Fraser, M. P., G. R. Cass, and B. R. T. Simoneit, Gas-phase and particle-phase organic compounds emitted from motor vehicle traffic in a Los Angeles roadway tunnel, *Environ. Sci. Technol.*, *32*, 2051–2060, 1998.

Fraser, M. P., M. J. Kleeman, J. J. Schauer, and G. R. Cass, Modeling the atmospheric concentrations of individual gas-phase and particle-phase organic compounds, *Environ. Sci. Technol.*, *34*, 1302–1312, 2000.

Gharib, S., and G. R. Cass, Ammonia emissions in the South Coast Air Basin, *Open File Rep. 84-2*, Environ. Qual. Lab., Calif. Inst. of Technol., Pasadena, 1984.

Gray, H. A., G. R. Cass, J. J. Huntzicker, E. Heyerdahl, and J. A. Rau, Characterization of atmospheric organic and elemental carbon particle concentrations in Los Angeles, *Sci. Total Environ.*, *36*, 17–25, 1984.

Griffin, R. J., D. Dabdub, and J. H. Seinfeld, Secondary organic aerosol, 1, Atmospheric chemical mechanism for production of molecular constituents, *J. Geophys. Res.*, *107*, 10.1029/2001JD000541, in press, 2002.

Harley, R. A., A. G. Russell, G. J. McRae, G. R. Cass, and J. H. Seinfeld, Photochemical modeling of the Southern California Air Quality Study, *Environ. Sci. Technol.*, *27*, 378–388, 1993.

Jacobson, M. Z., Development and application of a new air pollution modeling system, 3, Aerosol-phase simulations, *Atmos. Environ.*, *31*, 587–608, 1997.

Jacobson, M. Z., R. Lu, R. P. Turco, and O. B. Toon, Development and application of a new air pollution modeling system, 1, Gas-phase simulations, *Atmos. Environ.*, *30*, 1939–1963, 1996.

John, W., S. M. Wall, J. L. Ondo, and W. Winklmayr, Acidic aerosol size distributions during SCAQS: Report to the California Air Resources Board under Contract A6-112-39, Calif. Air Res. Board, Pasadena, 1990.

Kim, Y. P., J. H. Seinfeld, and P. Saxena, Atmospheric gas-aerosol equilibrium, I, Thermodynamic model, *Aerosol Sci. Technol.*, *19*, 157–181, 1993a.

Kim, Y. P., J. H. Seinfeld, and P. Saxena, Atmospheric gas-aerosol equilibrium, II, Analysis of common approximations and activity coefficient calculation methods, *Aerosol Sci. Technol.*, *19*, 182–198, 1993b.

Kleeman, M. J., and G. R. Cass, Identifying the effect of individual emissions sources on particulate air quality within a photochemical aerosol processes trajectory model, *Atmos. Environ.*, *33*, 4597–4613, 1999.

Kleeman, M. J., G. R. Cass, and A. Eldering, Modeling the airborne particulate matter complex as a source-oriented external mixture, *J. Geophys. Res.*, *102*, 21,355–21,372, 1997.

Lurmann, F. W., A. S. Wexler, S. N. Pandis, S. Musarra, N. Kumar, and J. H. Seinfeld, Modeling urban and regional aerosols, 2, Application to California's South Coast Air Basin, *Atmos. Environ.*, *31*, 2695–2715, 1997.

McRae, G. J., and J. H. Seinfeld, Development of a second-generation mathematical model for urban air pollution, 2, Evaluation of model performance, *Atmos. Environ.*, *17*, 501–522, 1983.

McRae, G. J., W. R. Goodin, and J. H. Seinfeld, Development of a second-generation mathematical model for urban air pollution, 1, Model formulation, *Atmos. Environ.*, *16*, 679–696, 1982.

Meng, Z., J. H. Seinfeld, P. Saxena, and Y. P. Kim, Atmospheric gas-aerosol equilibrium, IV, Thermodynamics of carbonates, *Aerosol Sci. Technol.*, *23*, 131–154, 1995.

Meng, Z., D. Dabdub, and J. H. Seinfeld, Chemical coupling between atmospheric ozone and particulate matter, *Science*, *277*, 116–119, 1997.

Meng, Z., D. Dabdub, and J. H. Seinfeld, Size-resolved and chemically resolved model of atmospheric aerosol dynamics, *J. Geophys. Res.*, *103*, 3419–3435, 1998.

Nguyen, K., and D. Dabdub, Two level time marching scheme using splines for solving the advection equation, *Atmos. Environ.*, *35*, 1627–1637, 2001.

Nguyen, K., and D. Dabdub, Semi-Lagrangian flux scheme for the solution of the aerosol condensation/evaporation equation, *Aerosol Sci. Technol.*, *36*, 407–418, 2002.

Pandis, S. N., A. S. Wexler, and J. H. Seinfeld, Secondary organic aerosol formation and transport, 2, Predicting the ambient secondary organic aerosol size distribution, *Atmos. Environ., Part A*, *27*, 2403–2416, 1993.

Pierson, W. R., A. W. Gertler, and R. L. Bradow, Comparison of the SCAQS tunnel study with other on-road vehicle emission data, *J. Air Waste Manage. Assoc.*, *40*, 1495–1504, 1990.

Pilinis, C., and J. H. Seinfeld, Continued development of a general equilibrium model for inorganic multicomponent atmospheric aerosols, *Atmos. Environ.*, *22*, 1985–2001, 1987.

Pun, B. K., R. J. Griffin, C. Seigneur, and J. H. Seinfeld, Secondary organic aerosol, 2, Thermodynamic model for gas/particle partitioning of molecular constituents, *J. Geophys. Res.*, *107*, 10.1029/2001JD000542, in press, 2002.

Robinson, R. A., and R. J. Stokes, *Electrolyte Solutions*, 2nd ed., Butterworths, London, 1965.

Rogge, W. F., M. A. Mazurek, L. M. Hildemann, G. R. Cass, and B. R. T. Simoneit, Quantification of urban organic aerosols at a molecular-level-identification, abundance and seasonal-variation, *Atmos. Environ., Part A*, *27*, 1309–1330, 1993.

Schauer, J. J., Source contributions to atmospheric organic compound concentrations: Emissions, measurements, and model predictions, Ph.D. thesis, Calif. Inst. of Technol., Pasadena, 1998.

Schauer, J. J., M. J. Kleeman, G. R. Cass, and B. R. T. Simoneit, Measurement of emissions from air pollution sources, 1, C_1 through C_{29} organic compounds from meat charbroiling, *Environ. Sci. Technol.*, *33*, 1566–1577, 1999a.

Schauer, J. J., M. J. Kleeman, G. R. Cass, and B. R. T. Simoneit, Measurement of emissions from air pollution sources, 2, C_1 through C_{30} organic compounds from medium duty diesel trucks, *Environ. Sci. Technol.*, *33*, 1578–1587, 1999b.

Schauer, J. J., M. J. Kleeman, G. R. Cass, and B. R. T. Simoneit, Measurement of emissions from air pollution sources, 3, C_1 through C_{29} organic compounds from fireplace combustion of wood, *Environ. Sci. Technol.*, *35*, 1716–1728, 2001.

Systems Applications International (SAI), User's guide for the urban airshed model, I, *Rep. SYSAPP-90/018a*, San Rafael, Calif., 1990a.

Systems Applications International (SAI), User's guide for the urban airshed model, II, Preprocessors and postprocessors for the UAM modeling system, *Rep. SYSAPP-90/018b*, San Rafael, Calif., 1990b.

Systems Applications International (SAI), User's guide for the urban airshed model, III, The diagnostic wind model, *Rep. SYSAPP-90/018c*, San Rafael, Calif., 1990c.

Systems Applications International (SAI), User's guide for the urban airshed model, IV, The emissions preprocessor system, *Rep. SYSAPP-90/018d*, San Rafael, Calif., 1990d.

Systems Applications International (SAI), User's guide for the urban airshed model, V, Description and operation of the ROM-UAM interface program system, *Rep. SYSAPP-90/018e*, San Rafael, Calif., 1990e.

Wesely, M. L., Parameterizations of surface resistance to gaseous dry deposition in regional-scale numerical models, *Atmos. Environ.*, *23*, 1293–1304, 1989.

Wexler, A. S., F. W. Lurmann, and J. H. Seinfeld, Modeling urban and regional aerosols, I, Model development, *Atmos. Environ.*, *28*, 531–546, 1994.

Winner, D. A., and G. R. Cass, Modeling the long-term frequency distribution of regional ozone concentrations, *Atmos. Environ.*, *33*, 431–451, 1999.

D. Dabdub, Department of Mechanical and Aerospace Engineering, University of California at Irvine, Irvine, CA 92697-3975, USA. (ddabdub@uci.edu)

M. P. Fraser, Department of Civil and Environmental Engineering, Rice University, MS-318, P.O. Box 1892, Houston, TX 77251, USA. (mpf@rice.edu)

R. J. Griffin, Department of Civil and Environmental Engineering, Duke University, Box 90287, Durham, NC 27708-0287, USA. (robgriff@duke.edu)

M. J. Kleeman, Department of Civil and Environmental Engineering, University of California at Davis, 1 Shields Avenue, Davis, CA 95616, USA. (mjkleeman@ucdavis.edu)

J. H. Seinfeld, Department of Chemical Engineering and Division of Engineering and Applied Science, California Institute of Technology, Mail Code 210-41, 1200 East California Boulevard, Pasadena, CA 91125, USA. (seinfeld@caltech.edu)